
Article:
Asker, H., Rongong, J. orcid.org/0000-0002-6252-6230 and Lord, C. orcid.org/0000-0002-2470-098X (2018) Dynamic properties of unbonded, multi-strand beams subjected to flexural loading. Mechanical Systems and Signal Processing, 101. pp. 168-181. ISSN 0888-3270

https://doi.org/10.1016/j.ymssp.2017.08.028

DYNAMIC PROPERTIES OF UNBONDED, MULTI-STRAND BEAMS SUBJEUCTED TO FLEXURAL LOADING

Haval K. Asker*, Jem A. Rongong and Charles E. Lord

The University of Sheffield, Department of Mechanical Engineering

hkaasker2@sheffield.ac.uk

Abstract. Beam-like structures, constructed from many long strands that are constrained rather than bonded together, can provide appreciable levels of structural damping through friction between individual strands. This paper describes experimental and numerical studies, carried out on square-section metal beams, which are aimed at improving understanding of the relationship between construction and performance. A beam is formed from a pack of square-section strands that is held together at various compression loads with pre-calibrated clamps. Flexural deformation of the assembled beam is simulated using standard finite element analysis employing simple Coulomb friction at the interfaces. The validity of the assumptions used in the models is confirmed by comparison with three point bend tests on a regular nine strand construction at several different clamp loads. Dynamic loss factors for this beam are obtained by conducting forced vibration tests, which show that the damping is insensitive to frequency. Subsequent numerical studies are used to investigate the effects of increasing the number of strands whilst maintaining the overall cross-section geometry of the beam. It is found that the system stiffness drops and loss factor increases when more strands are used for a maintained beam cross-section. Interestingly, the energy dissipated by each beam construction is almost the same. These results provide a vital and necessary insight into the physics for stranded structures and materials that are largely prevalent in mechanical (e.g. cables) and electrical (e.g. wires) elements.

Keywords: friction; damping; multi-strand; loss factor; energy dissipation; three point bend

1 INTRODUCTION

It is usually desirable to have significant levels of damping in machinery and structures to control resonant vibrations. Devices incorporating dry metal friction can provide useful levels of damping over a large range of operating temperatures and are therefore of considerable interest in a number of different industry sectors. This study examines the dissipation of energy through dry friction that occurs between mating contact surfaces within unbonded, multi-strand

beams. Current examples of this type of structure include fibre optic cables, wire rope dampers and composite materials where fibre wetting is incomplete.

The frictional damping mechanism has been used to control vibrations for many years. In the 1950s Goodman and Klumpp [1] considered the use of dry slip damping for reducing resonant vibrations in gas turbine blades. As part of this work, a quasi-static hysteresis loop was obtained experimentally and compared with a mathematical model in which the area of the hysteresis loop was used to calculate the energy dissipation. This concept was also utilized to calculate the frictional energy dissipation in a system with a lap joint contact [2, 3].

When a damped structure is subjected to cyclic loading, a phase difference exists between the stress and the strain (or force and displacement). When these terms are plotted against one another, a hysteresis loop is formed. This hysteresis loop can be used to determine the vibrational loss factor, η, which is a measure of the damping of the structure. The loss factor depends on the ratio of the energy dissipated per cycle, W_d, to the maximum strain energy induced by the cyclic deformation, U_{max}, according to Equation 1.

$$\eta = \frac{W_d}{2\pi U_{max}} \tag{1}$$

The presence of dry friction causes nonlinear behaviour in vibrating systems. This is because the friction force, which acts in the opposite direction to the motion, is constant in magnitude irrespective of the motion amplitude. Where the contribution of dry friction to the overall damping levels is significant, the loss factor is therefore dependent on the vibration amplitude as is the effective stiffness and hence the resonance frequency [4–6].

The widespread availability of finite element (FE) analysis has enabled an increased use of parametric studies to investigate and explain the behaviour of friction dampers under non-trivial geometric and loading conditions. When used in conjunction with experimental studies, they can provide quantitative, full-field information not easily obtained in an experiment. For example, Chen and Deng [7] found that a FE model was able to replicate the slip damping observed in the classical models of Goodman and Klumpp [1] and of Metherell and Diller [8]. FEs have also been used to study the frictional damping behaviour of unbonded multi-layer beams [9, 10]. This has included a direct comparison of the hysteresis behaviour obtained both numerically and by physical experiment which showed that the static spring rate gave good agreement [11].

This paper considers the flexural deformation of multi-strand beams. As the beam flexes, if the load is large enough, slip between individual strands occurs along the length of the beam. This type of behaviour in a multi-strand beam is illustrated in Figure 1.

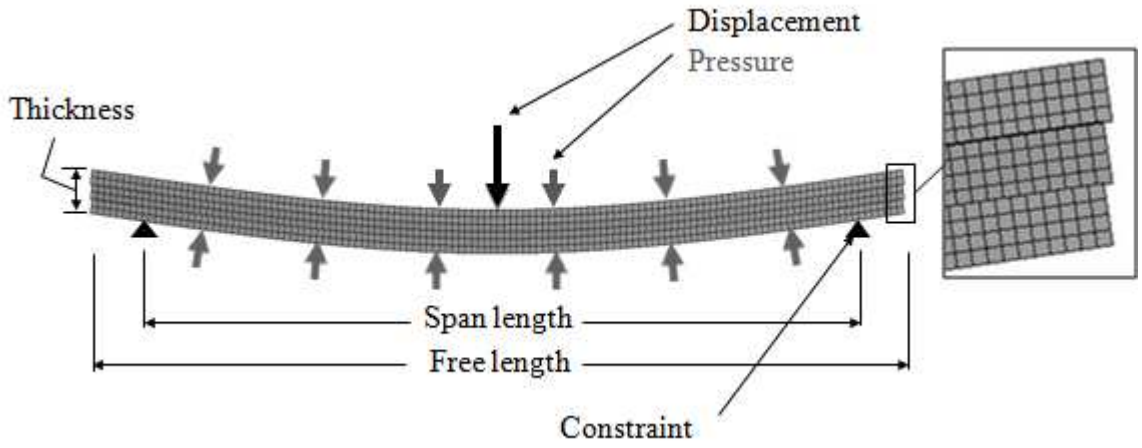

Figure 1: Typical multi-strand beam undergoing flexure (3×3 configuration)

The friction, and hence the energy dissipation, depends on forces acting perpendicular to the strand interfaces. Thus restraining mechanisms used to hold the strands together, for example clamps, have a crucial role in influencing the level of energy dissipation [12]. Researchers in the field of nanocomposites have also noticed the importance of friction between multiple thin strands and the surrounding matrix. The specific area, the ratio of surface area to the mass of the added nanomaterials, is often used as a measure of the extent of such interfaces within a particular composite and has been identified as a significant factor affecting the material loss factor. For example, Zhou et al [13] considered specific area when analysing the damping developed between carbon nanotubes and the matrix. They found that larger specific areas were associated with higher loss factor values. With regard to a multi-strand beam therefore, the indication is that a larger number of strands may increase damping levels providing that the same loading is applied.

The aim of this paper is to investigate the principal factors affecting the vibration of multi-strand beams. While the ability of such structural configurations to provide damping has been identified previously, an explanation of how performance is affected by design factors such as configuration, clamping pressure and loading conditions is not currently available. This work therefore, addresses the energy loss in multi-strand beams caused by dry friction when subjected to flexural loading. Physical tests and FE simulations are used to provide understanding that could be used by a designer seeking to create an optimised damper based on this mechanism.

2 METHODOLOGY

The beams studied in this work were constructed from nominally identical, square section steel strands, each 300 mm in length. To facilitate comparison between different strand arrangements, the overall dimensions of the beams were fixed at 300×12×12 mm. The configurations considered are defined in Table 1.

Configuration no.	Total no. of strands	Individual cross-sectional strand width and thickness, mm	No. of strands per row and column
1	4	6	2
2	9	4	3
3	16	3	4
4	36	2	6

Table 1: Multi-strand beam configurations

For each configuration considered, the energy dissipation and loss factor were obtained from the hysteresis loops generated from cyclic loading. This was achieved experimentally by performing three-point bend tests conducted first under quasi-static conditions and subsequently at several frequencies up to the first system resonance. As it was expected that behaviour would be dominated by sliding friction, results were obtained over several different amplitudes and clamping pressures.

The data from the quasi-static tests were used to validate a FE model that was then used for parametric studies. Note that the term quasi-static is used here to describe the situation in which changes to the applied loading occur over time periods that are significantly longer in duration than the period of any system resonances.

The main assumptions made in this work are as follows:

1. The principal energy dissipation mechanism is macroslip between adjacent strands. This can be adequately described by the Coulomb friction model.
2. Local stretching of individual strands is negligible.

Under these assumptions, the total compressive load applied perpendicular to an interface controls whether it undergoes macroslip or remains stuck irrespective of whether it is applied as a uniform pressure over the surface or at discrete points. Evidence to support this significant simplification, for situations where the compressive load is small relative to the stiffness of the system, is provided in the work of Damisa et al [14] and Lord [15]. Practically, this simplification was convenient as the strands were cut from lengths of extruded key steel with no further surface treatment (such as grinding) employed. This resulted in relatively inconsistent contact surfaces.

In numerical studies, compressive load was applied as a uniform pressure distributed over the outer surfaces of the beam. In the experimental work however, it was more convenient to use discrete clamps. These were designed to provide repeatable and accurate loading whilst minimising the overall size. The design also sought to minimise interference with motion in the

axial direction so that friction between beams was the only significant restriction to slip taking place. Each clamp comprised two semi-circular bars connected by bolts as shown in Figure 2.

The curved face of each clamp was pressed against the strands as the bolts were tightened, thereby providing the compressive clamp force. The curved face of each clamp provided a nominal line contact across the surface of the strands. With this design, it was assumed that energy dissipation arising from possible slip between the clamp and strands at the contact was much less significant than that occurring between the strands themselves. This is due to the shear stress (and hence likelihood of slip) being maximised at the centre of a beam under flexure and minimised at the top and bottom surfaces.

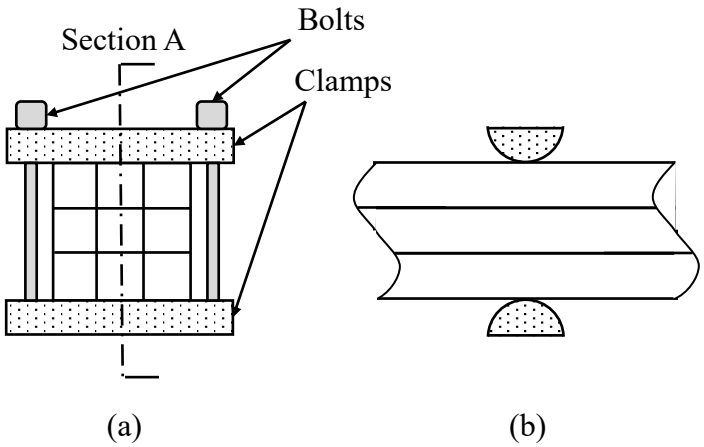

Figure 2: Clamp configuration on multi-stranded beam for (a) side view and (b) front view

The clamping force was applied as a torque to the bolts connecting the clamp halves. A test rig was used to measure the force from the applied torque. The test setup contained a load cell (Loadstar Sensor MFD-050-100) sandwiched between a pair of clamps. Various levels of torque were applied to the clamp bolts and the resulting force was measured. The tests were repeated five times and the average force for each torque level was taken as the nominal value for subsequent work. The results of the load-torque calibration experiments are shown in Figure 3.

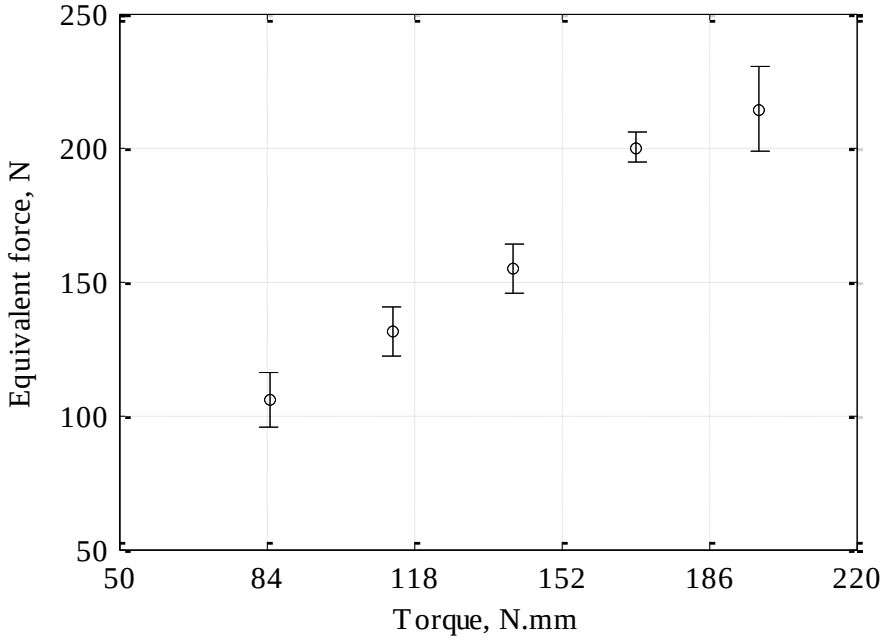

Figure 3: Equivalent clamping force values (error bars show one standard deviation)

Initially, when conducting the quasi-static loading tests, four clamps were used to provide clamping forces in the horizontal (width) and vertical (thickness) directions. However, it was found that the horizontal clamps had no effect on the overall result because the beam cross section was symmetrical about the loading direction. As a result, clamping was only applied in the vertical direction for the dynamic tests.

3 QUASI-STATIC EXPERIMENTS

Testing was carried out on a 9-strand beam comprising a 3×3 array of 4 mm strands (Configuration 2 in Table 1) using a three point bend arrangement. This beam was placed centrally between two stationary support rollers set 250 mm apart. Uniaxial loading was applied through a third non-rotating roller that was located centrally. All rollers had a diameter of 25 mm.

During testing, the strands were held together using discrete clamps, which were located approximately 50 mm from each of the support rollers. An image of the beam at the start of the three-point bend test, with the clamps attached, is presented in Figure 4.

Testing was carried out for different levels of clamping force and displacement amplitude. Loading was applied in the thickness direction through the loading roller using a servo-hydraulic test machine (MTS 858 Table Top System).

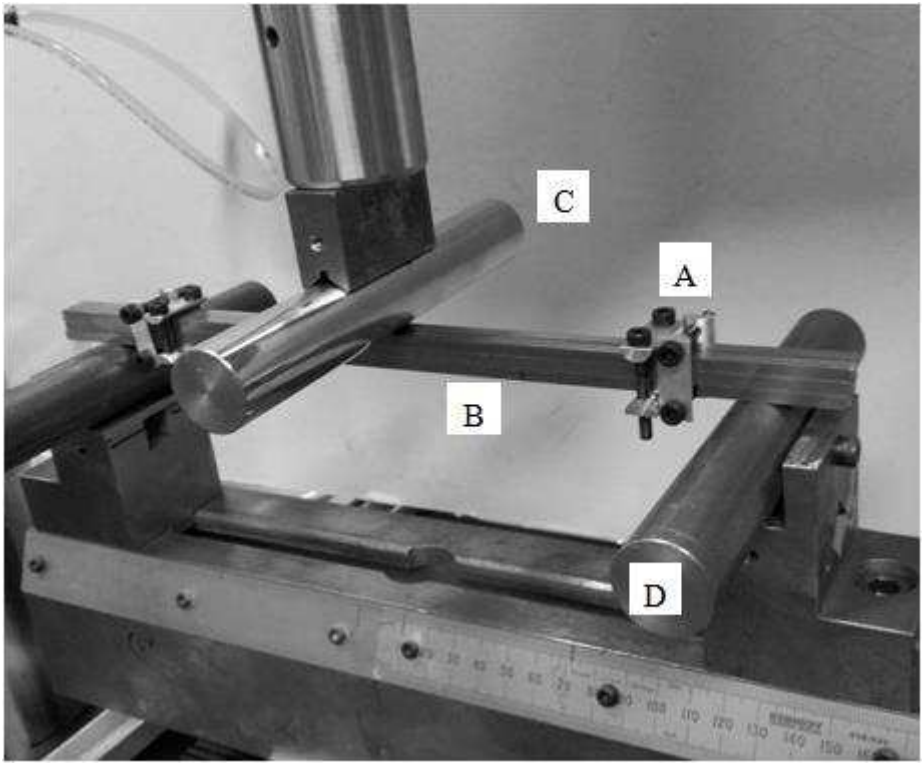

Figure 4: Test configuration showing (A) clamps, (B) beam, (C) loading roller and (D) support roller

At the start of each experiment, the loading roller was lowered until an initial contact (observed as an increase in the force signal) was made with the beam. From this point, the loading roller was lowered a further 0.1 mm to induce a light compressive load to ensure contact was maintained at all times between the loading roller and the beam. A sinusoidal displacement at a frequency of 1 Hz was then used to load the beam from the 0.1 mm initial displacement to additional peak-to-peak (PK-PK) displacements of 1.0 mm, 1.7 mm, and 2.5 mm. Testing was repeated at three levels of compression involving forces of 100 N, 190 N, and 250 N on each clamp.

To ensure operation within the elastic region for each strand, the maximum displacement was limited to 2.5 mm. At this deflection, the peak flexural stress was approximately 80% of the yield strength. After completing the tests at the maximum amplitude (2.5 mm), a test at the lowest amplitude (1.0 mm) was repeated and compared with the equivalent original test. In this way, it was found that significant permanent deflection did not occur in any of the strands.

Measured values of deflection and applied load for at least 14 cycles per loading condition were acquired during the test with a sample rate of approximately 100 Hz. Closed-loop control was employed to ensure that the displacement signal had a sinusoidal shape. The effect of friction between the strands could be seen in the force trace as a small phase difference (from damping) and a distortion of the waveform (from nonlinearity). A typical pair of signals is shown in Figure 5.

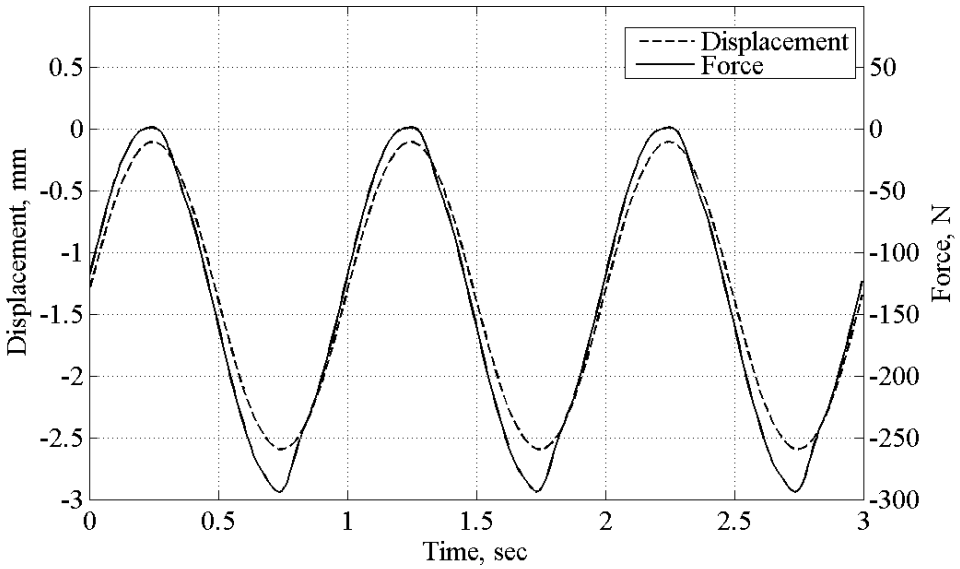

Figure 5: Force and displacement time histories with PK-PK amplitude 2.5 mm and clamp load 250 N

The corresponding force vs displacement hysteresis loop is shown in Figure 6. The loop shape is similar to those reported by others for dry friction hysteresis [16]. It can be seen that the shape is close to a parallelogram, which is what would be expected from a perfect system comprising a linear spring and Coulomb friction in series. For the measured loop, zones dominated by different contact conditions are highlighted in Figure 6: segments AB and CD are macroslip, while BC and DA are nominally stuck. In an idealised model, the segments BC and DA would be parallel and the transition to macroslip would be sharp. In the experiment, these zones are curved and have different gradients indicating that some microslip does occur. However, it can be seen that the system is dominated by macroslip and hence the assumptions made in this work remain acceptable.

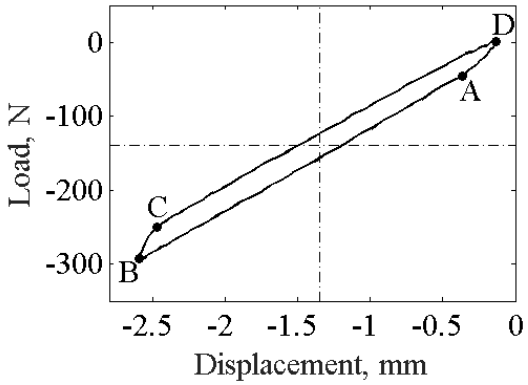

Figure 6: Hysteresis loop for Configuration 2 at PK-PK amplitude of 2.5 mm with zones identifying principal friction conditions

An interesting secondary observation that can be made in Figure 6 is that the loop is thicker under high load (left hand side of the plot) than under low load. An explanation for this is that the load applied during testing, which at maximum deflection is of a similar magnitude to the total clamping load, also increases the contact pressure and hence the point at which macroslip begins.

The measured hysteresis loops were used to obtain the system properties, which are summarised for each condition in Table 2. The procedure for obtaining these properties has been discussed in the literature [17-19] and is briefly outlined below.

1. The energy dissipated per cycle was computed from the area enclosed within a hysteresis loop.
2. The underlying nonlinear load-deflection curve (excluding energy dissipation) was obtained by averaging force levels obtained during loading and unloading for given deflection values. The stiffness at a given deflection was then calculated from the gradient of the load-deflection curve at that position.
3. The strain energy was given by the area under the nonlinear load-deflection curve. As this was needed to calculate the loss factor (which is a vibration property), the curve was first re-centred around the mean displacement position which was designated as the nominal equilibrium position. This is identified by the chain lines in Figure 6.
4. The system loss factor was then obtained from the energy dissipation and the effective peak strain energy. As the load-deflection curve was not symmetric about the mean displacement position, the strain energy values at extreme displacements were not equal. Instead, U_{max} in Equation 1 was taken as the average between these values.

Configuration2		Energy dissipation per cycle, mJ	Effective peak strain energy, mJ	Stiffness, N/mm	Loss factor
Displacement PK-PK, mm	Clamp force, N				
1	100	6.72	14.0	113	0.08
1	190	10.9	13.9	110	0.12
1	250	19.0	14.3	111	0.21
1.7	100	17.0	40.1	113	0.07
1.7	190	25.7	40.1	113	0.10
1.7	250	41.1	40.7	111	0.16
2.5	100	33.9	85.7	112	0.06
2.5	190	46.5	85.7	112	0.09
2.5	250	71.9	86.6	111	0.13

Table 2: System properties of beam Configuration 2 under various loading and clamping conditions

At each loading condition, small fluctuations were noticed during the first few cycles. As it was unclear whether this was caused by a physical process or a feature of the hydraulic machine

controller, these cycles were ignored. Results were instead, averaged from the last ten cycles of each test condition.

Examination of Table 2 shows that loss factors increased with clamp force but reduced with displacement amplitude. This behaviour is as expected, because for all clamping and loading conditions investigated, the hysteresis loop resembled a long, thin parallelogram (as shown in Figure 6). As the dominant mechanism affecting energy dissipation is macroslip, the contribution of the ends is minimal. Under these conditions, the loss factor is effectively proportional to the thickness of the loop divided by the displacement range. Thus, a larger clamp force increases the thickness of the loop by retarding the onset of slip, while increased displacement makes it proportionally thinner. Clearly, if the clamp force becomes too large, macroslip is reduced or eliminated and the exact shape of the loop ends (which are affected by microslip) would become significant. At extreme loads, all relative motion would cease and energy dissipation would be negligible [15].

4 DYNAMIC EXPERIMENTS

Dynamic experiments were used to investigate the sensitivity of the loss factor to vibration frequency. While the same beam configuration as for quasi-static tests was used, some changes to the test arrangement were required to allow the use of an electrodynamic shaker (500 N peak sine force) rather than the hydraulic test machine used previously of particular significance was that the signal generator and shaker-amplifier system could not support a constant load and therefore loading had to be applied both sides of the true equilibrium position. The test setup is shown in Figure 7 and a brief description is given below.

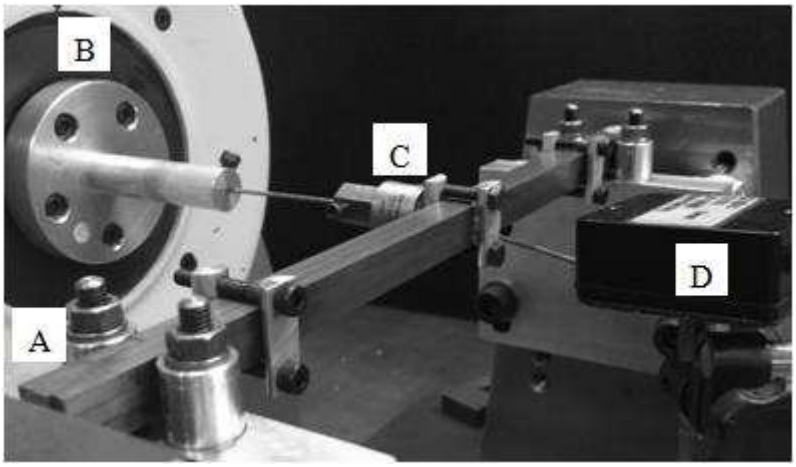

Figure 7: Set-up for the dynamic experiment with: (A) support rollers, (B) electrodynamic shaker (LDS V455), (C) force sensor (Dytran 1053V3), (D) laser displacement sensor (MicroEpsilon LD1605-10).

The strands comprising the beam were compressed in the direction of excitation using two clamps placed 55 mm from each end of the beam. The torque on the bolts was set so that the

clamping force applied by each clamp was 250 N (i.e. a total force of 500 N over the beam). A third clamp, attached at the midpoint of the beam, was connected to the shaker via a transversely flexible “stinger” and a force sensor. This clamp was only used to connect the shaker to the beam; hence, bolts were tightened enough to avoid relative motion between the beam midpoint and the shaker but not enough to have a significant effect on the overall clamp force.

The beam was placed between two pairs of support rollers in order to mimic a simply supported boundary. Each roller pair held the beam with sufficient pressure to stop the beam from dropping onto the roller holders during testing. Again, this pressure was kept to a minimum to avoid significant changes to the overall clamp force. The distance between the roller pairs, i.e. the span of the beam, was set at 250 mm.

The system was excited using sinusoidal waveforms with frequencies in the range 10 Hz to 200 Hz. The motion of the central clamp, and hence the midpoint of the beam, was measured using a laser displacement sensor. A closed-loop controller was used to maintain constant displacement amplitude at each frequency. The layout of the instrumentation and signals is provided in Figure 8.

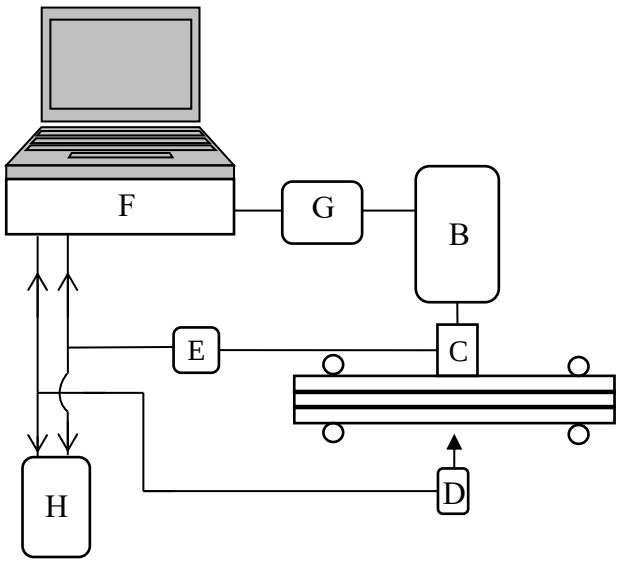

Figure 8: Instrumentation layout for the dynamic experiment with (B)-(D) as Figure 7, (E) signal conditioning unit (F) controller (SigLab20-22A), (G) 1 kW power amplifier (H) oscilloscope (Picoscope4424)

At each frequency of interest, force and displacement signals were acquired at a sampling rate of 50 kHz over a period of 2 seconds. During testing, some high frequency noise was noticeable, particularly on the displacement reading. This was attributed primarily to the surface roughness at the laser measurement point and, at higher amplitudes, possible slip at the support rollers and in the clamp used to connect the shaker. To remove these effects, the force and displacement signals were isolated using a fast Fourier transform based filter that rejected spectral components with frequencies greater than 25 times the test frequency or below 5 Hz. This relatively large pass-band was employed to ensure that important harmonics arising from the

nonlinear response were not excluded: it was observed that the excluded spectral components had magnitudes that were three orders of magnitude lower than the fundamental.

A plot showing the receptance frequency response function (FRF) at different amplitude levels is provided in Figure 9. The figure also shows best-fit curves obtained using equivalent linear single degree-of-freedom (SDOF) system models. The parameters of these models are provided in Table 3. From these results, it can be seen that the system stiffness and damping reduced as the dynamic amplitude increased. This softening behaviour for a friction system is in line with observations made by others [6, 16].

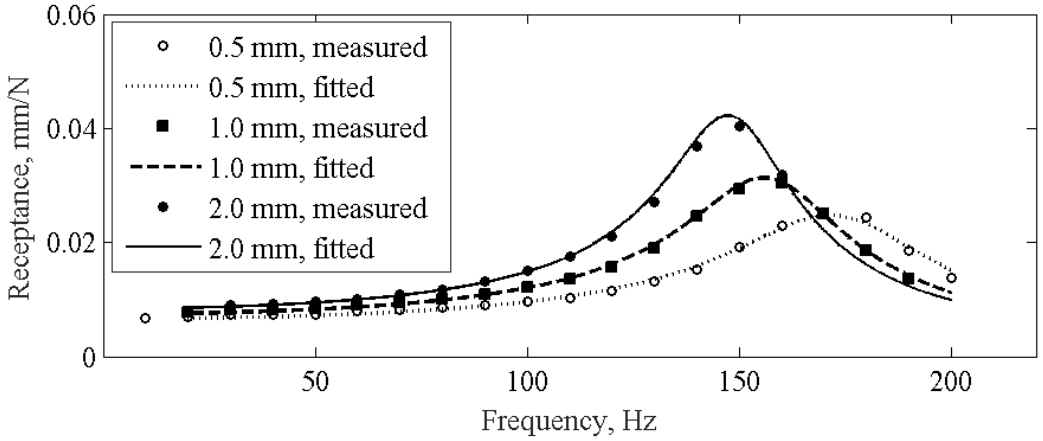

Figure 9: Receptance for a clamp force of 250 N per clamp for PK-PK displacement amplitudes of 0.5 mm, 1 mm and 2 mm

PK-PK amplitude, mm	Natural frequency, Hz	Damping ratio	Effective mass, kg
0.5	174.7	0.13	0.125
1.0	158.2	0.12	0.136
2.0	148.8	0.10	0.136

Table 3: Natural frequency parameters at PK-PK displacement amplitudes of 0.5 mm, 1.0 mm and 2.0 mm

The nonlinear behaviour was also investigated by examining the hysteresis loops at each frequency. In order to do this, inertia effects first had to be removed from the measured force signal f_{meas} using,

$$f = f_{meas} + \omega^2 x m_{eff} \quad (2)$$

where x is the measured displacement, ω the frequency of excitation in rad/s and m_{eff} the effective mass (from the SDOF curve fits). Note that the sign in Equation 2 is positive because the inertia term is 180° out of phase with the displacement. Figure 10 shows examples of the

hysteresis loops obtained from the experiments for different PK-PK excitation displacements and frequencies.

It can be seen, for the parameters considered, that all of the excitation levels achieve macroslip. As the excitation amplitude is increased, the beam extends into the macroslip region increasing the energy dissipated along with the peak strain energy. Importantly these increase at different rates therefore making the loss factor nonlinear with respect to the amplitude.

Figure 11 shows the loss factors (obtained from the SDOF fit to the receptance curve) for the full range of frequencies considered at PK-PK displacements of 0.5 mm, 1 mm, and 2 mm respectively. The vertical line in each plot shows the system natural frequency. It can be seen that for all displacements, the loss factor remains relatively constant and close to the value indicated by the receptance curve fit (note that the curve fit used a viscous damping model but at resonance, the equivalent system loss factor is twice the damping ratio).

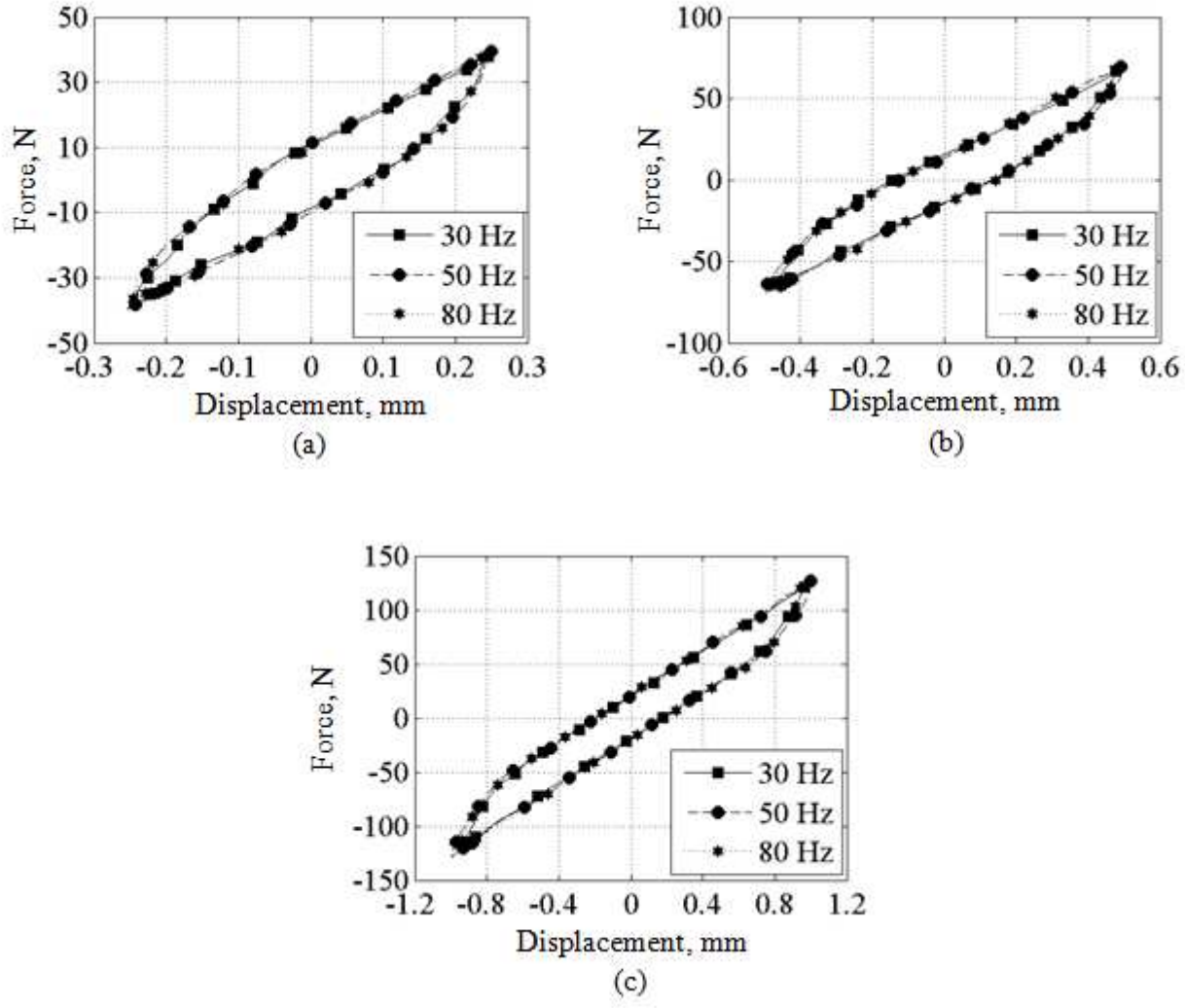

Figure 10: Hysteresis loop at different frequencies with PK-PK displacement amplitudes of (a) 0.5 mm, (b) 1 mm and (c) 2 mm

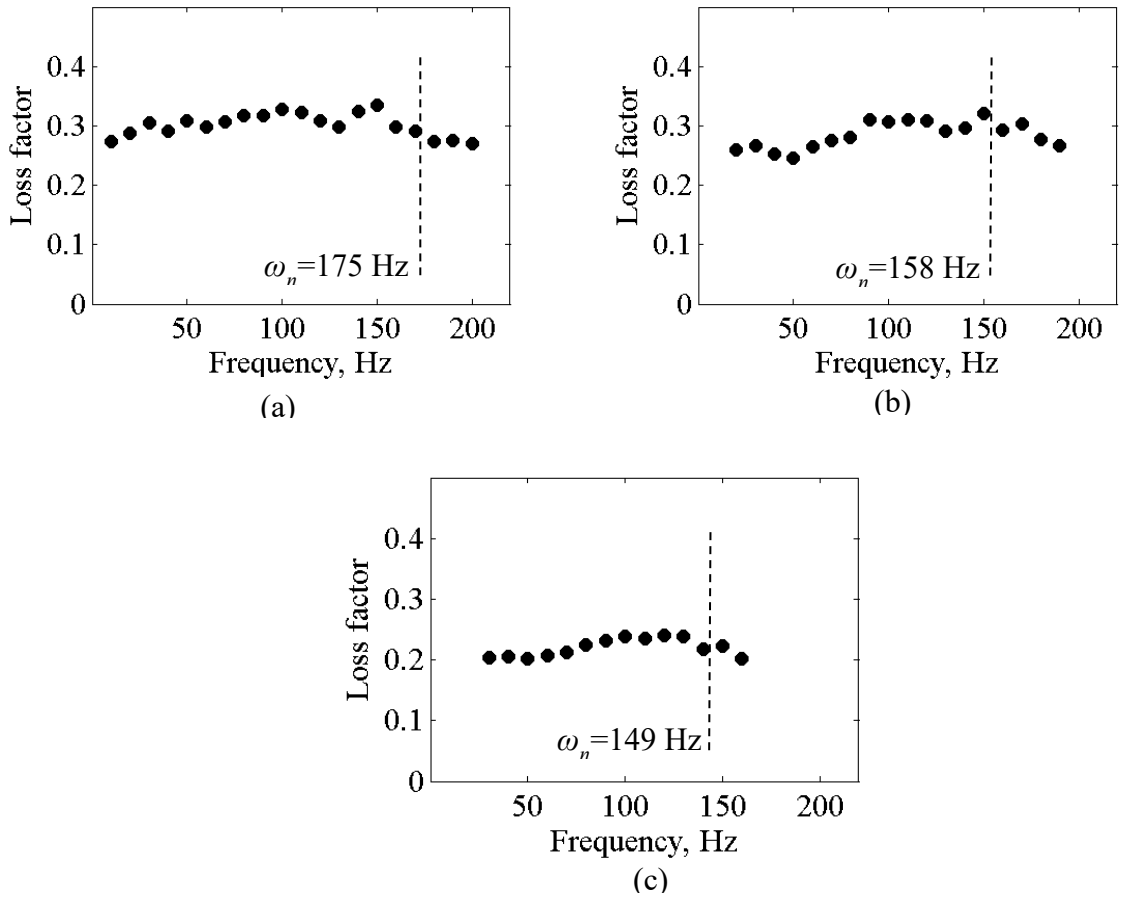

Figure 11: Loss factor values over a range of excitation frequencies with PK-PK displacement amplitudes of (a) 0.5 mm, (b) 1 mm and (c) 2 mm

Figure 12 presents the energy dissipation per cycle over the range of excitation frequencies for PK-PK displacements of 0.5 mm, 1 mm, and 2 mm respectively. While the values remain reasonably close, there is some fluctuation caused by differences in actual amplitude of vibration (the controller achieved amplitude accuracy to within 10%) and possibly distortion caused by higher harmonics that were evident at higher frequencies. The effect of the applied (shaker) load on the contact pressure may also have been significant here. This is because this applied load would have been in-phase with the displacement at low frequencies, retarding the onset of slip (and thereby increasing energy loss) but at resonance, this force would be 90 degrees out of phase with the displacement, and therefore would not affect the onset of macroslip significantly.

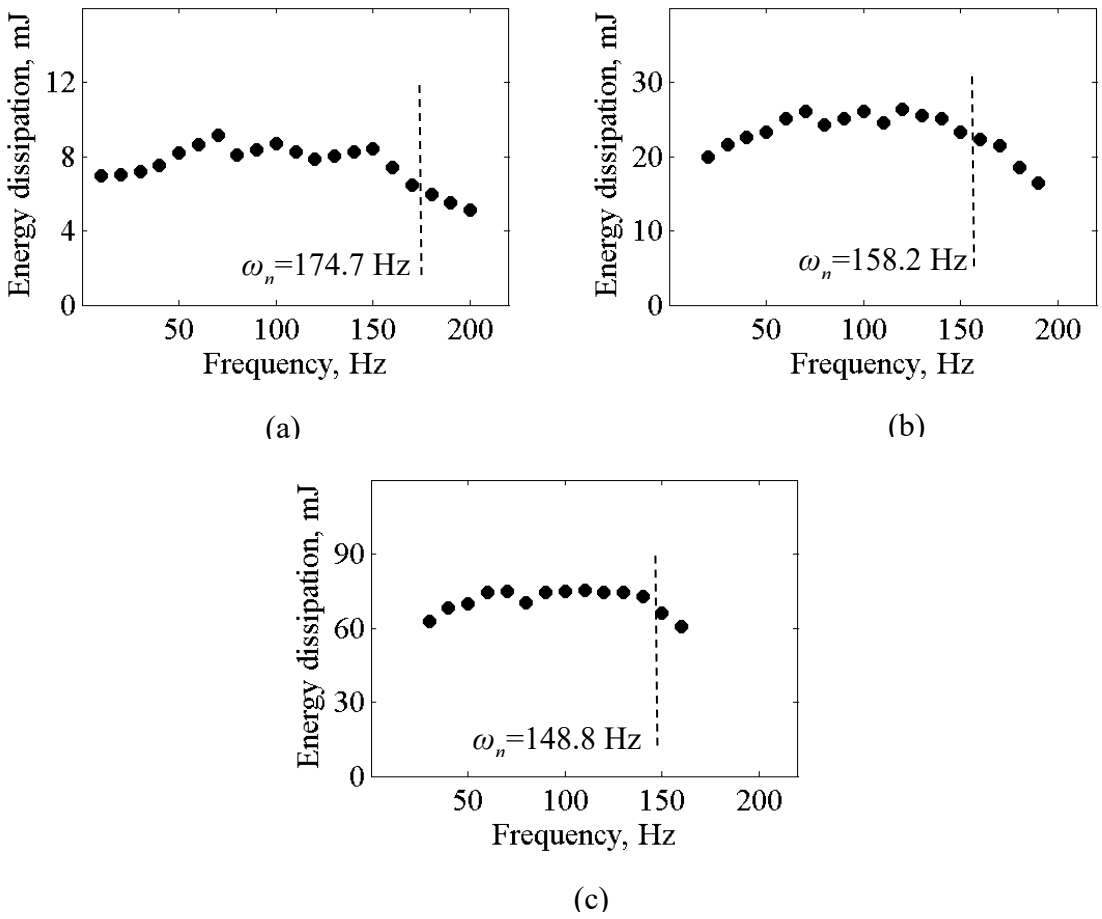

Figure 12: Energy dissipation per cycle over a range of excitation frequencies with PK-PK displacement amplitudes of (a) 0.5 mm, (b) 1 mm and (c) 2 mm

5 QUASI-STATIC NUMERICAL ANALYSES

Quasi-static and dynamic test results indicated that macroslip occurring between strands was the main energy dissipation process. Finite element (FE) analysis was also carried out to provide further understanding of multi-strand beams.

Models were made for Configurations 1-4 from Table 1. Important material properties for the key steel strands were obtained in earlier work [17] and hence measurement methods are not described here in detail. The strands were considered to have linear elastic properties with Young's modulus of 190 GPa (obtained from the natural frequency of single strands) and Poisson's ratio 0.3 (typical for steel). The dynamic coefficient of friction used at the interfacial surfaces was 0.25 – a value obtained for the key steel specimens using a test rig developed by Lord [15].

Modelling was conducted using the commercial software ANSYS. Each strand was modelled with 20 node quadratic brick elements while the interaction between each interface was modelled with 8-node surface-surface contact (CONTA174) and 3-D, target segment

(TARGE170) elements. A Coulomb friction model was used where sliding occurs if the tangential force exceeds the limiting force defined as the product of normal force and coefficient of friction. The number of potential slip zones meant that convergence was not easily achieved. To help with this, an augmented Lagrange contact formulation was used along with a contact stiffness factor of 0.075. This value was selected to minimise penetration whilst achieving convergence and was obtained by running calculations on several contact stiffness factors in the range 0.001-0.1. The maximum penetration for the chosen contact stiffness factor was 0.136 µm, which is an order of magnitude less than the typical roughness of drawn steel, so was considered unlikely to be significant. The element size was approximately 1 mm, which resulted in a model with 36000 elements. As the level of discretisation significantly exceeded the expected deformation pattern, extensive mesh convergence studies were not required. Instead, validation was achieved though comparisons made directly with experimental results.

Each configuration was constrained and loaded as a beam subjected to three-point flexure (see Figure 1) with a sinusoidal load as in the quasi-static experiments detailed in Section 2. Numerical results were compared with the data from the quasi-static experiments. The clamping force was simulated as a uniform pressure along both the outer-upper and outer-lower surfaces of the beam as this was found to be more convenient than applying point loads at the clamp locations. To provide consistency with earlier experimental work, the term "clamp force" is still used but it should be noted that the contact force generated by the pressure was the same as the contact pressure generated by two clamps: thus, a clamp force of 250 N is represented as a pressure of 0.139 MPa.

The force-displacement hysteresis loops were compared between the experimental and numerical results as these provide information on both stiffness and energy dissipation. A comparison with clamp forces of 100 N, 190 N and 250 N are shown in Figures 13-15 for displacements of 1.0 mm, 1.7 mm and 2.5 mm, respectively.

There is close agreement between the experimental and numerical results: the difference in root mean square (RMS) values for numerical and experimental force signals were found to be less than 4% and are listed in Table 4.

Clamp force, N	RMS difference %		
	PK-PK Displacement, mm		
	1.0	1.7	2.5
100	1.30	0.76	0.07
190	3.96	1.82	1.45
250	3.30	1.36	1.20

Table 4: Root mean square difference between numerical and experimental force signal

The results from the comparison between the experimental and numerical hysteresis loops show that the FE model adequately represents the experimentally obtained force-displacement behaviour for the multi-strand beams. Dynamic tests have shown that results are relatively insensitive to frequency. Thus, it can be inferred that a quasi-static FE model can be used to estimate the vibration damping properties of a multi-strand beam. This close agreement is attributed to the fact that macroslip dominates the response and slip velocities are relatively low (estimated from the modelled deformation to be below 50 mm/s even for the tests at 200 Hz).

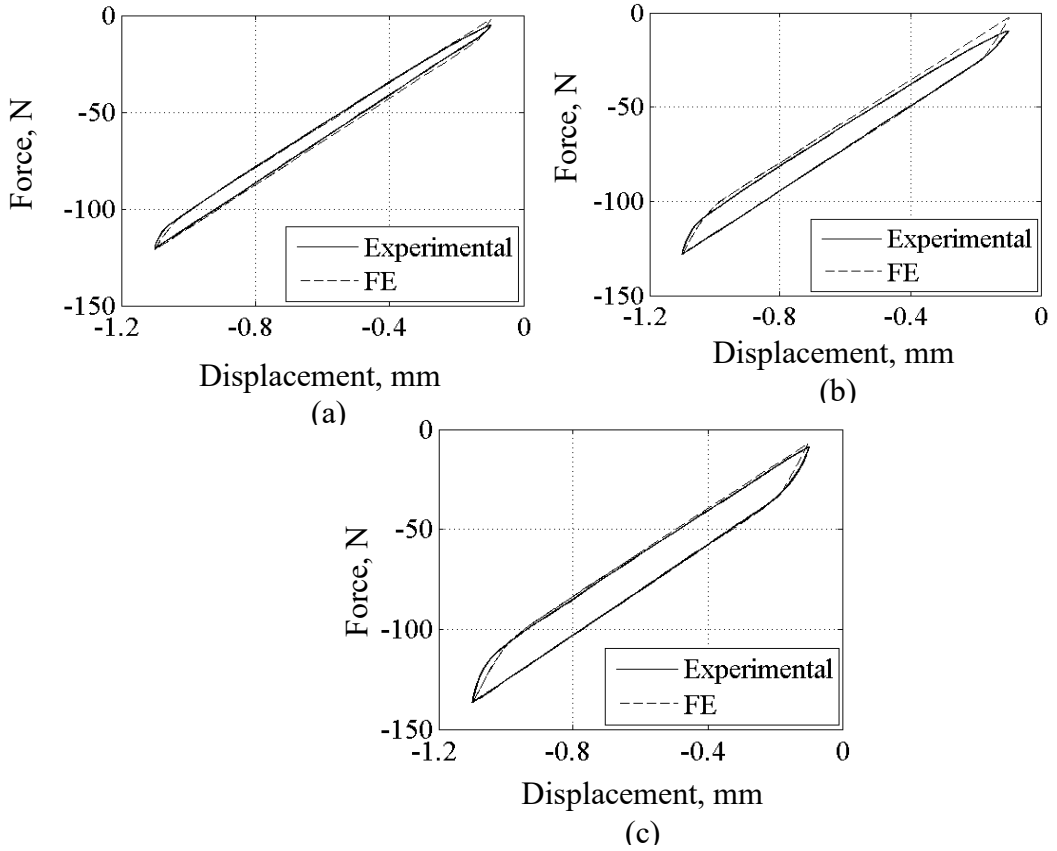

Figure 13: Comparison of experimental and numerical hysteresis loops for a sinusoidal displacement waveform with amplitude of 1.0 mm and clamp force of (a) 100 N. (b) 190 N. (c) 250 N

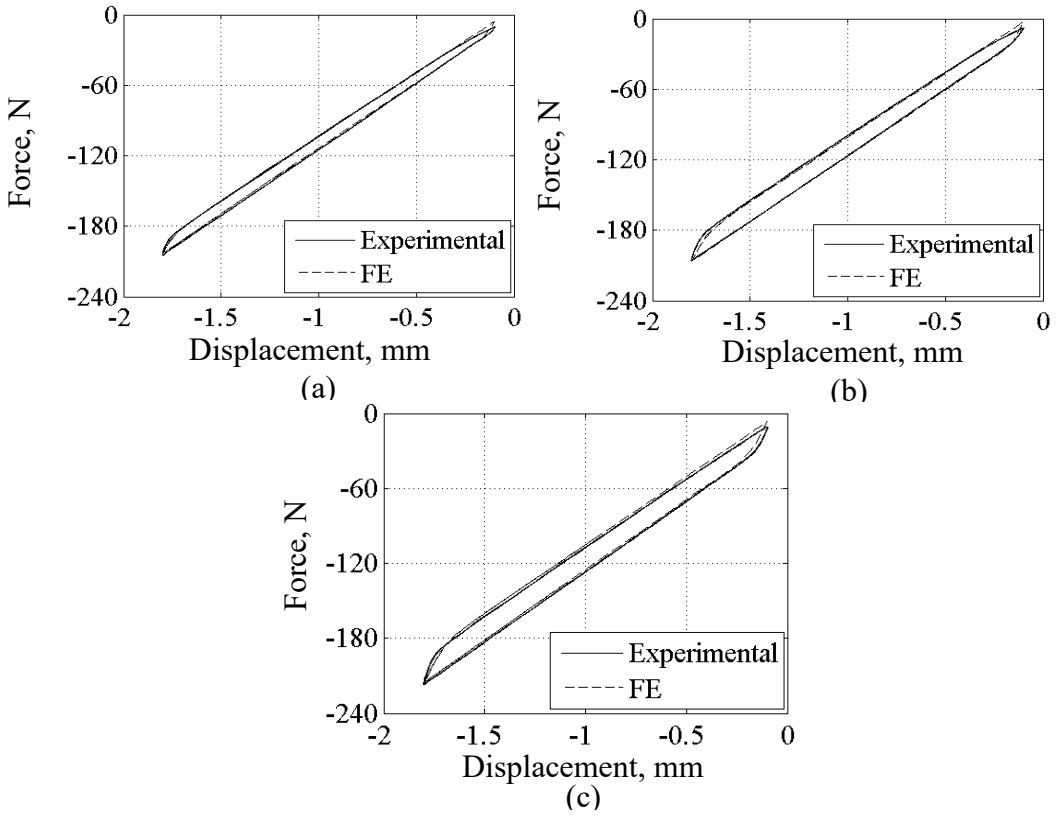

Figure 14: Comparison of experimental and numerical hysteresis loops for a sinusoidal displacement waveform with amplitude of 1.7 mm and a clamp force of (a) 100 N. (b) 190 N. (c) 250 N

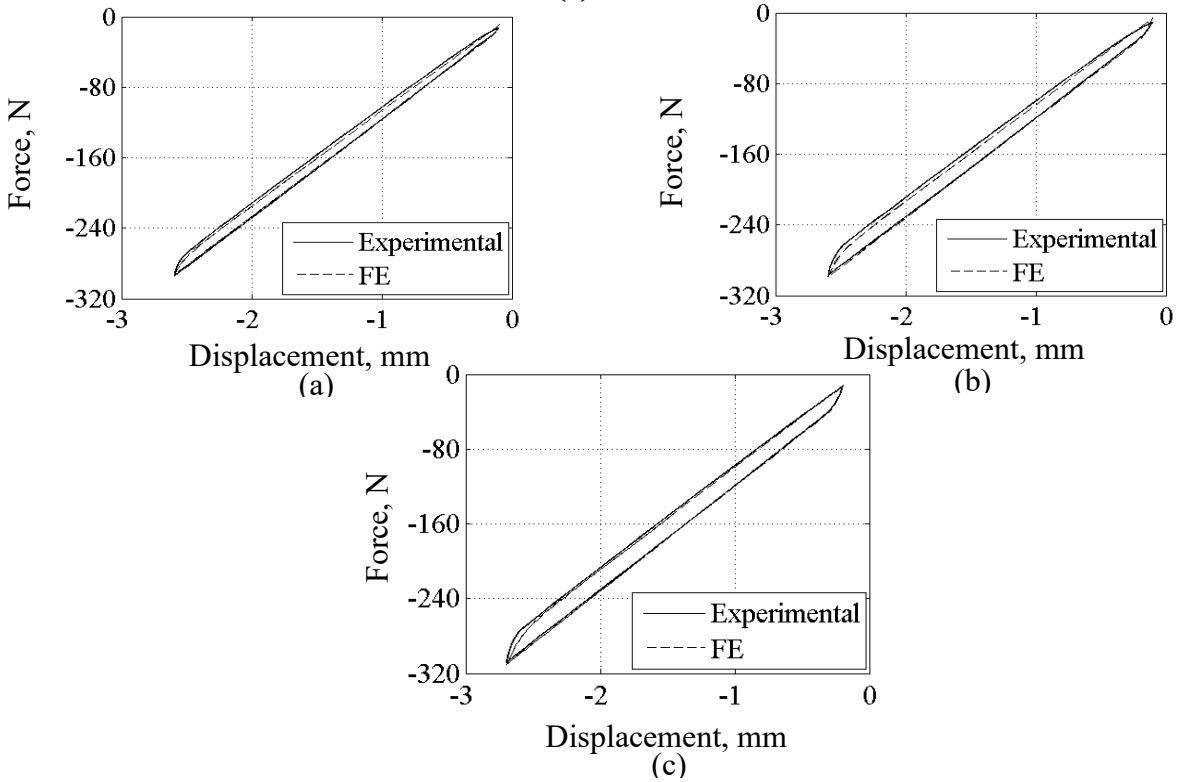

Figure 15: Comparison of experimental and numerical hysteresis loops for a sinusoidal displacement waveform with amplitude of 2.5 mm and a clamp force of (a) 100 N. (b) 190 N. (c) 250 N

Using the validated FE model, a comparison was made between the numerical force-displacement hysteresis loops generated for Configurations 1-4 when subjected to a clamp force of 250 N and a sinusoidal displacement of 1.0 mm. Hysteresis loops are presented in Figure 16 while the resulting energy dissipation and loss factor values are shown in Figures 17 and 18 respectively. In these simulations, the overall cross-sectional area of the beam, the modulus of elasticity of individual strands, and the coefficient of friction between the strands did not change.

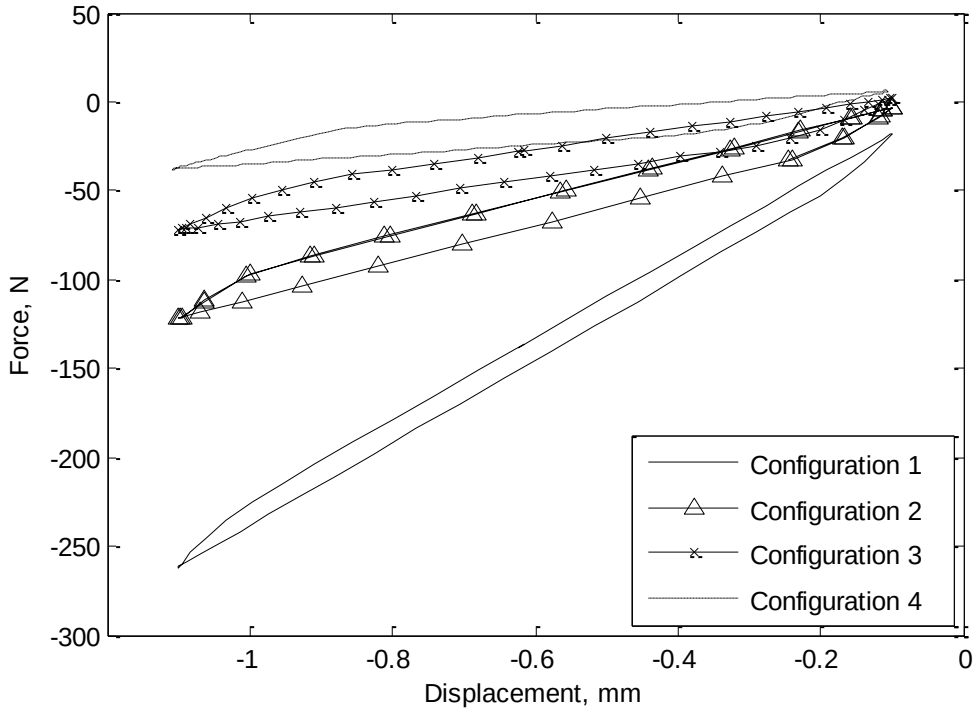

Figure 16: Numerical force-displacement curves for four different multi-strand beam configurations

From Figure 16 it can be observed that increasing the number of strands reduces the gradient of the hysteresis loop and hence the effective system stiffness. This can be explained by considering the zero-friction condition where the total stiffness of the square strand array is simply the sum of the stiffness values of each individual strand – i.e. the second moment of area is given by,

$$I_{\mu=0} = \frac{t_{beam}^4}{12n^2} \qquad (2)$$

where n is the number of strands and t_{beam} the thickness of the beam. Therefore, a beam comprising many small strands stores less energy than one with a few large ones. The ends of the hysteresis loops can be seen to change somewhat as the number of strands increases. This is because there are more interface layers. As shear stress is highest at the beam centreline, slip occurs first on parallel interfaces nearest to the neutral axis. As the load and displacement is increased, the critical condition for slip is reached at interfaces further away. This rather than

one transition between stick and slip, the beam experiences several. This provides the apparent extension of the "curved" end of the hysteresis loop.

Figure 17 shows the energy dissipation (per cycle) for different numbers of strands and clamp forces. It can be seen that this value does not change dramatically as the number of strands increases. The likely reason for this is that the normal clamp force and the total deflection remain unchanged. The sensitivity to clamp force has already been noted in previous sections.

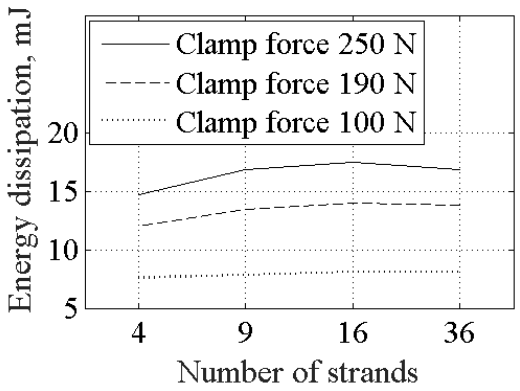

Figure 17: Relationship between the energy dissipation, clamp force, and number of strands for Configurations 1-4 at 1.0 mm PK-PK displacement

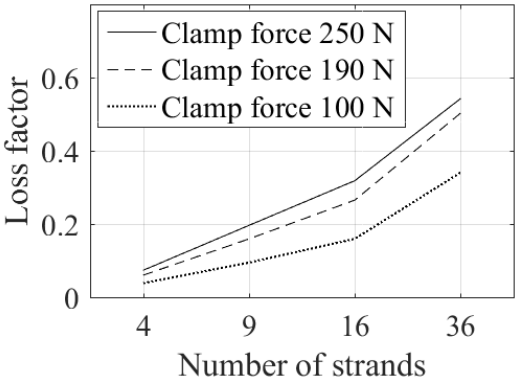

Figure 18: Relationship between the loss factor, clamp force, and number of strands for configurations 1-4 at 1.0 mm PK-PK displacement

Figure 18 shows the equivalent variation of loss factor. Because the dissipated energy remains approximately the same and the stiffness (and therefore the ability to store strain energy) reduces as the number of strands increase, the loss factor increases with the number of strands. This increase is not linear and the level of nonlinearity increases as the clamp force increases.

6 CONCLUSIONS

In this paper it has been shown that for a multi-strand beam undergoing flexural deformations at given amplitude, the total energy dissipated per cycle remains more-or-less the same, no matter how many strands are used provided that the overall cross-section of the bundle remains unchanged. A larger number of strands results in a more flexible structure that stores less energy

for a given displacement. The loss factor therefore increases with the number of strands in the system.

The dynamic behaviour of the loss factor in a multi-strand beam was addressed. The main conclusion that can be drawn from the data presented is that the loss factor can be considered independent of frequency for the conditions experienced. The beam was found to be highly nonlinear and its natural frequencies were dependent on the level of excitation. For the parameters considered in this paper, the loss factor decreased when the applied displacement increased and this behaviour was clear in both the quasi-static and dynamic experiments.

REFERENCES

[1] L.E. Goodman, J.H. Klumpp, Analysis of slip damping with reference to turbine blade vibration, J. Appl. Mech. 23 (1956) 421–429.

[2] S. Earles, Theoretical estimation of the frictional energy dissipation in a simple lap joint, J. Mech. Eng. Sci. 8 (1966) 207–214.

[3] Z. Qin, D. Cui, S. Yan, F. Chu, Hysteresis modeling of clamp band joint with macro-slip, Mech. Syst. Signal Process. 66–67 (2016) 89–110. doi:10.1016/j.ymssp.2015.04.038.

[4] A.A. Ferri, Friction damping and isolation systems, J. Vib. Acoust. 117 (1995) 196–206. doi:10.1115/1.2838663.

[5] W.E. Whiteman, A.A. Ferri, Displacement-dependent dry friction damping of a beam-like structure, J. Sound Vib. 198 (1996) 313–329.

[6] E. Chatelet, G. Michon, L. Manin, G. Jacquet, Stick/slip phenomena in dynamics: Choice of contact model. Numerical predictions & experiments, Mech. Mach. Theory. 43 (2008) 1211–1224. doi:10.1016/j.mechmachtheory.2007.11.001.

[7] W. Chen, X. Deng, Structural damping caused by micro-slip along frictional interfaces, Int. J. Mech. Sci. 47 (2005) 1191–1211. doi:10.1016/j.ijmecsci.2005.04.005.

[8] A.F. Metherell, S. V Diller, Instantaneous energy dissipation rate in a lap joint — uniform clamping pressure, ASME J. Appl. Mech. 35 (1968) 123–128.

[9] H.M. Sedighi, K.H. Shirazi, K. Naderan-Tahan, Stick-slip analysis in vibrating two-layer beams with frictional interface, Lat. Am. J. Solids Struct. 10 (2013) 1025–1042.

[10] H.M. Sedighi, K.H. Shirazi, K. Naderan-Tahan, Stick-slip vibrations of layered structures undergoing large deflection and dry friction at the interface, J. Vib. Acoust. 135 (2013) 61006-1-61006–12. doi:10.1115/1.4024218.

[11] Y. Yum, Frictional behavior of automotive leaf spring, Proc. 4th Korea-Russia Int. Symp. Sci. Technol. Ulsan, South Korea,. 3 (2000) 5–10.

[12] Y.K. Ponomarev, Control of damping for multi-layer vibration insulators with dry friction on contact surfaces, Int. J. Eng. Technol. 6 (2014) 2225–2228.

[13] X. Zhou, E. Shin, K.W. Wang, C.E. Bakis, Interfacial damping characteristics of carbon nanotube-based composites, Compos. Sci. Technol. 64 (2004) 2425–2437. doi:10.1016/j.compscitech.2004.06.001.

[14] O. Damisa, V.O.S.. Olunloyo, C.A.. Osheku, A.A. Oyediran, Static Analysis of Slip

Damping With Clamped Laminated Beams Static Analysis of Slip Damping with Clamped Laminated Beams, JEuropean J. Sci. Res. 17(4) (2007) 455–476.

[15] C. Lord, Damping Effects of Debonded Composites, PhD Thesis, The University of Sheffield, 2012.

[16] N. Zhou, T.K. Ghosh, On-line measurement of fabric-bending behaviour: background, need and potential solutions, Int. J. Cloth. Sci. Technol. 10 (1998) 143–156.

[17] H. Asker, J. Rongong, C. Lord, Mathematical and numerical evaluation of the damping behaviour for a multi- strand bar, in: EACS 2016 – 6th Eur. Conf. Struct. Control., 2016: pp. 1–10.

[18] K. Chandrasekhar, J.A. Rongong, E.J. Cross, Frequency and amplitude dependent behaviour of tangled metal wire dampers, Int. Conf. Noise Vib. Eng. (2014) 559–572.

[19] H.K. Asker, J.A. Rongong, C.E. Lord, Stiffness and loss factor of unbonded , multi-strand beams under flexural deformation, in: Int. Conf. Eng. Vib., Ljubljana, Slovenia, 2015: pp. 1518–1529.